# Large scale simulation of high pressure water mist systems

T. Sikanen, J. Vaari & S. Hostikka
*Fire and Evacuation Safety, VTT Technical Research Centre of Finland*

## Abstract

Water mists systems are used to protect people and property from fires. They suppress fires by three main mechanisms: removal of heat from the gases, displacement of oxygen by water vapour and attenuation of radiation by droplets. Correct prediction of these mechanisms hinges on accurate modeling of droplet transport. This paper discusses the modeling and simulation of high speed water mist systems using Large Eddy Simulation and a Lagrangian description of the spray. The focus is on the droplet transport. Particular attention is given to the droplet injection model and sub models for coupling of the dispersed and continuous phases. Effects of turbulence modeling on droplet transport is explored. The modeling results are compared to experimental data from both small and large scale experiments.
*Keywords: water mist, interphase momentum transfer, turbulence modeling, large eddy simulation, lagrangian-eulerian,large scale.*

## 1 Introduction

Water mist systems are widely used to protect people and property from fires and are increasingly being used for projects that are significantly larger than the scale of experimental testing. The demonstration of the effectiveness of large scale water mist systems then calls for large scale simulations of these systems. The multiscale nature of large scale water mist systems presents many problems simulations. Due to aerodynamic drag, individual fine water droplets will decelerate quickly in the surrounding air even if their initial velocity is high. High pressure water mist nozzles often consist of a number of micronozzles, each discharging a relatively narrow jet. When the jet entrains surrounding air, the fine droplets in the core of the jet will not experience significant drag, and can therefore be transported far


WIT Transactions on Engineering Sciences, Vol 79, 
www.witpress.com, ISSN 1743-3533 (on-line)
doi:10.2495/MPF130071

away from the discharge orifice. Depending on the nozzle design, individual jets may or may not interact with each other. In the former case, relatively narrow spray patterns are produced with a good penetration far into the protected space. In the latter case, wider patterns are produced allowing larger nozzle spacing and good spray coverage in shallow spaces. Ability to accurately model spray dynamics is therefore crucial whenever it is desired that the design of water mist systems could be aided with simulations.

This paper focuses on issues of large scale water mist system simulations. Several authors have looked at Computational Fluid Dynamics simulation of water mist in the past. Prasad *et al.* [1, 2] and Shimizu *et al.* [3] studied extinguishment of small scale fires by water mist using two-fluid models. Two-fluid models were also used by Prasad *et al.* [1,2] and Nmira *et al.* [4] to study extinguishment by water mist in large enclosures and tunnels, respectively.

Kim and Ryou [5, 6] used the Fire Dynamics Simulator (FDS) version 3.0 for modeling fire suppression of pool fires by water mist in steel enclosure. Hart [7] used Fluent and a Lagrangian spray model to study fire suppression by water mists. An extensive study of water mist modeling by CFD was done by Husted [8] in his PHD Thesis. He used FDS version 4.0 and compared predictions to experimental measurements. This paper uses data from large scale water mist experiment to identify problems in the Eulerian-Lagrangian methods when applied with structured CFD. Some possible solutions are also presented.

## 2 Description of computational tools

### 2.1 Gas phase

The Fire Dynamics Simulator (svn revision 15001) is used in this study. The governing equations and solution methods for the gas phase are described in the FDS Technical Reference Manual [9] and will not be repeated here. FDS uses Large Eddy Simulation to describe the turbulent motion of the gas phase and Lagrangian description of the dispersed phase. Equally spaced cartesian meshes are used in all simulations in this paper.

### 2.2 Lagrangian particle model

Ignoring buoyancy, lift and forces arising from fluid acceleration, the motion of a single spherical droplet is governed by the equation of motion

$$\frac{dm_p\vec{v}_p}{dt} = F_p; \qquad F_p = m_p\vec{g} + \rho_g C_D \pi r_p^2 \left(\vec{v}_p - \vec{v}_g\right) \left\|\vec{v}_p - \vec{v}_g\right\| \tag{1}$$

Here on the left hand side $m_p$ is the mass of the droplet and $\vec{v}_p$ is the velocity of the droplet. On the right hand side, $\vec{g}$ is the gravitational acceleration, $\rho_g$ is the density of the surrounding gas, $\vec{v}_g$ is the velocity of the surrounding gas, $r_p$ is the radius of the droplet, and $C_D$ is the drag coefficient. The drag coefficient is given

by [9]

$$C_D = \begin{cases} Re/24 & Re < 1 \\ \frac{Re}{24}\left(1 + 0.15Re^{0.683}\right) & 1 < Re < 1000 \\ 0.44 & Re > 1000 \end{cases} \quad (2)$$

where $Re = 2\,\|\vec{v}_p - \vec{v}_g\|\,r_p/\nu$ is the droplet Reynolds number and $\nu$ is the kinematic viscosity of air. Due to the large number of droplets in a real spray, only a fraction of these droplets is tracked. Each droplet in the simulation represents a parcel of droplets with the same properties. The number of droplets in the simulation is controlled by droplet insertion rate parameter. Unless otherwise mentioned this rate parameter was set to $5{\cdot}10^5$ droplets per second.

To ensure that the momentum lost by the droplets is distributed correctly in the gas, an additional CFL-like condition can be placed on the global time step. The global time-step of the numerical solver is adjusted according to

$$\Delta t \leq C min\left(\frac{v_x}{\Delta x}, \frac{v_y}{\Delta y}, \frac{v_z}{\Delta z}\right), \quad (3)$$

where $C$ is a user defined constant between 1 and 0, and $v_x$, $v_y$, and $v_z$ are the three components of the particle velocity $\vec{v}_p$. All sprays considered in this paper are non-evaporating.

### 2.3 Interphase momentum transfer

The momentum transfer between droplets and the gas phase is modeled via source a term in the momentum equation. Correct estimation of the distribution of this source term is vitally important for correct simulation of multiphase flows. Several methods have been proposed, see e.g. [10] and [11]. The most commonly used method is the Particle In Cell (PIC) method that assigns the momentum from a droplet to the nearest gas phase velocity node.

We adopt a method based on kernel density estimation. Kernel estimates of density are weighted averages of point values over a neighbourhood

$$\mathcal{F}\left(\vec{x}\right) = \sum_i K\left(\vec{x_i}, \vec{x}\right) F_i. \quad (4)$$

Here the summation is over all particles in the simulation.On the right hand side $\mathcal{F}$ represents force density and $F_i$ are the forces from individual droplets.. In practise, only a subset of all the particles in the neighbourhood of the evaluation point is considered. In this paper, the kernel is taken to be a truncated gaussian kernel

$$K\left(\vec{x_i}, \vec{x}\right) = \begin{cases} \frac{1}{\pi\sqrt{\pi}h^3}\exp\left[-\frac{\|\vec{x_i}-\vec{x}\|^2}{h^2}\right] & \|\vec{x_i} - \vec{x}\| \leq 2h \\ 0 & \|\vec{x_i} - \vec{x}\| > 2h \end{cases} \quad (5)$$

The width parameter $h$ is taken to be equal to the grid spacing. To get the total force acting on a grid node, integral of the density over a grid cell (volume) is

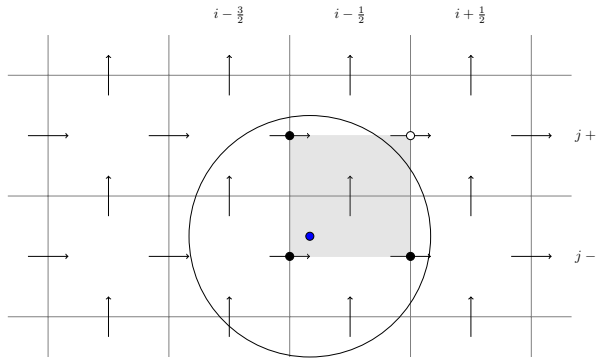


Figure 1: Staggered grid and evaluation points for the density interpolator.

needed. This integral can be approximated as an average of the corner values of the staggered cube. For example, for y-momentum at cell $ijk$ we have:

$$F_{y,ijk} \approx \frac{1}{8}\Big[\mathcal{F}_{y,i-1\ j-\frac{1}{2}\ k} + \mathcal{F}_{y,i-1\ j-\frac{1}{2}\ k} + \mathcal{F}_{y,i-1\ j+\frac{1}{2}\ k} + \mathcal{F}_{y,i\ j+\frac{1}{2}\ k} + \mathcal{F}_{y,i\ j+\frac{1}{2}\ k-1} + \mathcal{F}_{y,i\ j-\frac{1}{2}\ k-1} + \mathcal{F}_{y,i-1\ j+\frac{1}{2}\ k} + \mathcal{F}_{y,i\ j-\frac{1}{2}\ k}\Big]\Delta x\Delta y\Delta z. \tag{6}$$

After this averaging, the force terms $F_{ijk}$ are scaled so that the total momentum received but the gas phase equals that lost by the droplets. Fig. 1 illustrates the interpolation and averaging points. The blue dot represents the particle and the gray rectangle shows the staggered grid cell surrounding a y-momentum node. The circle shows the neighborhood of a gaussian kernel centered at the particle position. For the remainder of this paper the momentum transfer method described here will be referred to as SPH.

## 3 Spray boundary condition

The flow rate of a spray head can be calculated from its flow constant K. The flow constant K is defined as

$$Q = K\sqrt{p}, \tag{7}$$

where $Q$ is the flow rate of water, and $p$ is the water pressure measured at the spray head.

The initial position of a particle is picked randomly within the conical section of a spherical surface. The surface is located distance $l$ from the nozzle location and is delineated by the spray angle $\theta$. A variable flux density within the spray is implemented by defining a probability density function for the initial position.The

Table 1: Simulation parameters for the single orifice nozzle used in this study.

| $K\left(L/\min atm^{1/2}\right)$ | $\theta$(deg) | $d_m(\mu\text{m})$ | $\gamma$ |
|---|---|---|---|
| 0.433 | 12 | 79 | 2.26 |

joint probability of the initial latitude and longitude is

$$p(\theta,\varphi) = p(\theta)\,p(\varphi) = \frac{1}{2\pi}\sin\theta f(\theta). \tag{8}$$

An exponential shape function is used to place more mass in the center of the spray.

$$f(\theta) = \exp\left[-\beta\left(\frac{\theta-\theta_{\min}}{\theta_{\max}-\theta_{\min}}\right)^2\right] \tag{9}$$

The spread parameter $\beta = 5$ was used in this work. All the droplets are given the same initial speed in the direction of the surface normal.

It is assumed that all the atomization processes are over at the position of boundary condition. In the simulations the cumulative volume fraction (CVF) of droplet size is assumed to follow a mixture of Rosin-Rammler and log-normal distributions

$$F(d) = \begin{cases} \frac{1}{\sqrt{2\pi}}\int_0^d \frac{1}{\sigma d'}\exp\left[-\frac{\left[\ln\left(d'/d_m\right)\right]^2}{2\sigma^2}\right]dd' & d \le d_m \\ 1-\exp\left[-0.693\left(\frac{d}{d_m}\right)^{\gamma}\right] & d > d_m \end{cases} \tag{10}$$

Here $d_m$ is the volumetric median diameter, while $\sigma$ and $\gamma$ are width parameters. The width parameters are related by $\sigma = 1.15/\gamma$ to ensure continuity at $d_m$.

The median droplet size is known to depend on the operating pressure used. When needed, this variation in droplet size is taken into account by scaling the median droplet size as $d_m \sim p^{-1/3}$. In all the simulations initial droplet velocities were calculated from

$$v_0 = 0.95\sqrt{\frac{2p}{\rho_l}}, \tag{11}$$

where $p$ is the operating pressure of the nozzle and $\rho_l$ is the density of the liquid. Factor 0.95 was used to account for the friction losses in the nozzle.

The multiorifice spray-head considered in this paper is modeled by positioning several single orifice models with different orientations at one point in the computational domain. Each individual orifice on the nozzle was modeled with the parameters given in Table 1. The center nozzle points in the axial direction and the eight perimeter nozzles are equally spaced and at a 45 degree angle in relation to the center nozzle.

## 4 Description of validation experiments

The experimental data used to validate the simulation results comes from to different experimental campaigns. In one set of experiments, single water mist nozzle orifice were characterized. The data was obtained by the Direct Imaging (Shadowgraphy) technique, and it consisted of size distribution, velocity,mist flux and particle concentration at several locations across the spray cone. The measurement locations were those defined in the NFPA 750 standard and an additional measurements point on the center line of the cone. The center line measurement point was added because otherwise the dense core of the sprays would have been missed. All the measurements were made at 70 bar operating pressure.

The second set of validation data comes from a large scale water distribution experiment. The water distribution measurements were conducted in the large test hall of VTT Fire Technology. The hall has a floor area of 14 m $\times$ 27 m and a maximum height of 18 m for a gross volume of 6000 $m^3$. The spray heads were mounted on a steel support at 2 m height above the floor level. They were aligned along the centerline of the longer dimension of the hall, and spraying horizontally.

Of primary interest in the experiment was the horizontal distribution of the water spray on the floor level along the spray axis, which was measured using five 1m by 1m rectangular steel trays. In each of the nine tests, water was discharged for 30 minutes to collect a sufficient amount of water in each container. After end of discharge, the amount of water in each container was measured with a relative accuracy of better than 10%. Water distributions were measured for three spray heads and with three pressures for each spray heads. However, in this paper we only consider one spray-head and one pressure. Results were similar for all pressures and spray heads. More complete descriptions can be found in the report [12].

## 5 Simulation results

### 5.1 Near field simulations

The nozzle characterization experiments were modeled using a rectangular computational area 1.5 m high, 0.5 m wide and 0.5 m deep. The computational area was open to flow on all sides. The nozzles were placed 0.1 m from the top of the computational domain and the measurements were taken 1 meter below the nozzle.The simulation results correspond to droplet properties averaged over a sphere with 1 cm radius centered at the measurement location. The number of Lagrangian particles used to describe the sprays was approximately $3{\cdot}10^4$. Timesteps in the simulations varied from 400 microsecond for the 4 cm grids to 100 microseconds for the 1 cm grids.

Fig. 2 compares predicted droplet velocities with experimentally measured ones. In Fig. 2a) the PIC method is used, while in Fig. 2b) shows results with the SPH method. In both cases the velocity on the spray centerline is over predicted.

Somewhat surprisingly, the predicted velocities are faster for the simulation utilizing SPH. The convergence of the velocities is also slower. For the PIC method, differences between 1 cm grid and 2 cm grid are negligible on the spray centerline.

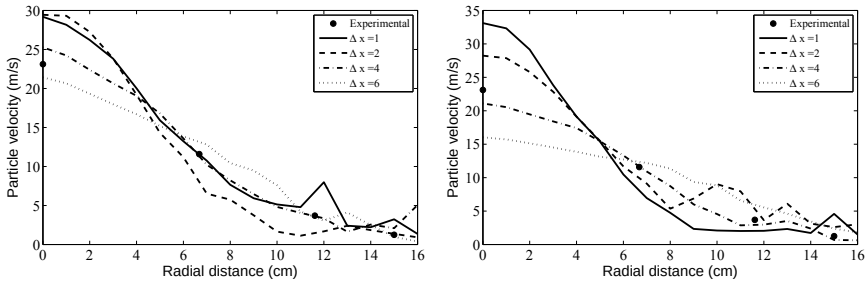


Figure 2: Grid sensitivity analysis for single orifice mist nozzle. In a) the original PIC method is used. In b) the SPH method is used.

### 5.2 Large scale simulations

In the simulations only a small section of the large test hall is simulated. The simulation domain is 16 meters long 9.6 meters wide and 5 meters high. All boundaries except the floor are set open to flow. The experiments ran for 30 minutes, while only 30 seconds are simulated. The spray head is positioned 2 meters from the floor and one meter away from the nearest open boundary. In the experiments, the spray head was attached to a metal back plate and this metal back plate was included in the computational model. The grid spacing used here is 4 centimeters. The computational area was split into twelve 4 meter long 3.3 meter wide and 5 meter high meshes.

Fig. 3 presents results from simulation of large scale water distribution tests. The experimental data is from pans placed on the spray centerline. The simulation results correspond to area integrals of accumulated water at the locations of the square basins. The simulation results are scaled to account for the simulation time that was shorter than the actual experiment time.

It is obvious that the water distribution is heavily concentrated directly in front of the spray head. Fig. 3b) shows 5m/s velocity isosurfaces directly in front of the spray head. It can be seen that the gas jets driven by the orifices on the perimeter dissipate much quicker than the central jet.

The small water mist droplets created at the orifices behave as tracer particles very soon after leaving the nozzle. Thus the particles are transported only as far as

the gas jet will carry them. When the jets dissipate, around 2 meters away from the nozzle, the particles drop almost straight down under the influence of gravity.

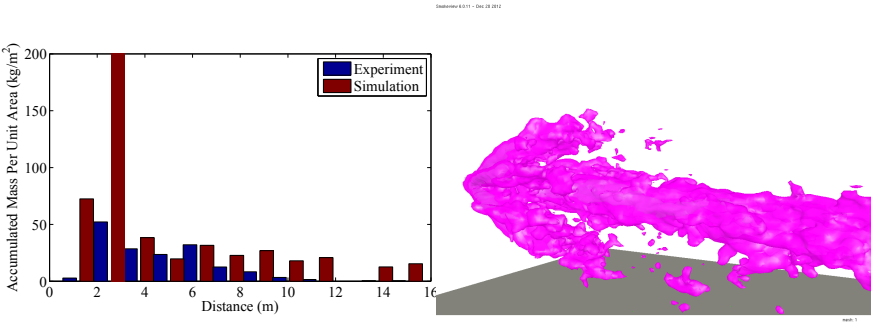


(a) (b)

Figure 3: a) Comparison of simulation results with experimental data for water distribution in large hall experiments. b) 5 m/s velocity isosurface in front of the nozzle.

### 5.3 Simulation of oblique spray jets

The problem encountered in the large scale simulations stems from difficulties in simulating non-grid-aligned (oblique) sprays. First problem is that, on a coarse grid, the momentum source terms near the nozzle will be differently distributed in the oblique and grid-aligned cases. The second problem has to do with simulation of turbulence although the exact mechanism is still unclear.

First, we compare results from simulations of oblique spray jets with results from simulations of grid aligned spray-jets. The computational for the grid aligned jets model is the same near field simulation model that was used in Section 5.1. for simulation of oblique jets a computational domain 2 meters in length, 1 meter in width 2 meters high is used. In this simulations, the spray is oriented at a 45 degree angle to the grid.

A sensitivity study was conducted to verify that the boundary conditions did not interfere with the results. Cubic domains with side lengths up to 8 meters, with the sprays positioned in the middle, were tested with no appreciable effect on the results. Tests were also run utilizing periodic and close and free slip boundary conditions and the differences between the angled and straight sprays remained. The droplet insertion rate was varied so that the number of droplets used to describe the spray varied between $50 \cdot 10^3$ and $500 \cdot 10^3$. Although the parameter is in itself important, increasing the number of droplets did not decrease the gap between the straight and angled cases.In short the effect described here is not very

sensitive to simulation parameters other than the grid size and turbulence model employed.

The first problem and its solution by using the interphase momentum transfer described in Section 2.3 is illustrated by Fig. 4a) and b). Clearly, smoothing the interphase momentum transfer terms produces better match between the centerline velocities in the oblique and grid aligned case. This effect is most noticeable on coarse grids. On finer grids the difference between the PIC and the SPH methods disappears. Grid convergence is not achieved with or without the new momentum transfer method. The second problem is related to turbulence modelling. Two

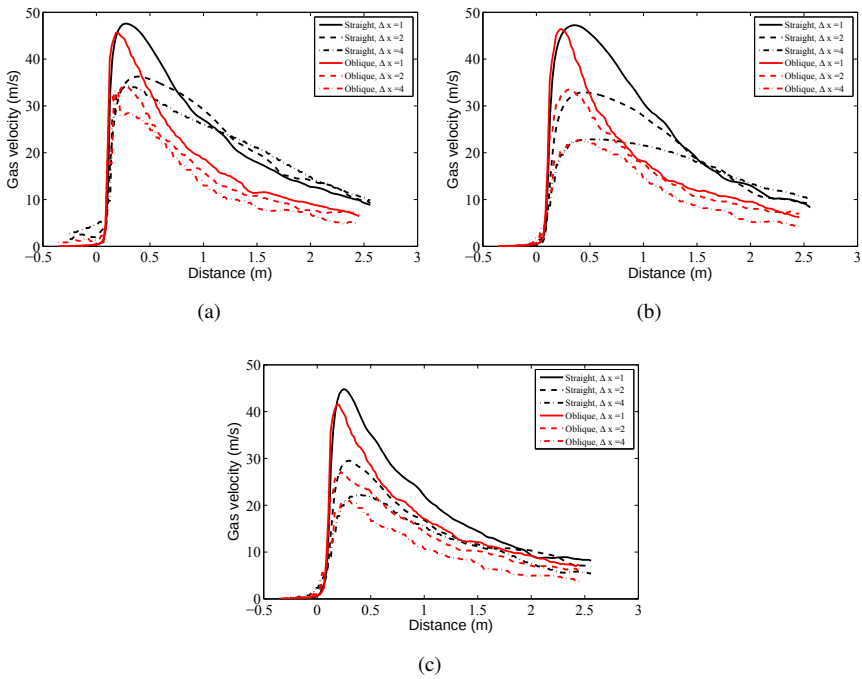


Figure 4: Effect of improved interphase momentum transfer method on average gas velocities on spray centerline. In figure a) default PIC method is used. In b) the SPH method is used In c) the dynamic Smagorinsky model is used in addition to the SPH method.

different models of turbulent viscosity are considered in the following. The dynamic Smagorinsky model [13, 14] and the Deardorff model [15]. To keep discussion brief only these two models are considered here

Fig. 4b) and c) show the gas velocities on the jet centerline for Deardorff and dynamic Smagorinsky models respectively. For both models the centerline velocity in the oblique case seems to attenuate faster than in the grid aligned case. There

are some notable differences between the results for the two turbulence models. For dynamic Smagorinsky model, the velocity for both oblique and grid aligned cases seems to decay at approximately the same rate. The velocity in the oblique case is however consistently lower than in the grid aligned case. For the Deardorff model, the velocity decay is much faster in the oblique cases. Furthermore, for coarse grids, the velocity decay in the grid aligned case is almost linear, further enhancing the differences between the spray directions. On a 1 cm grid the velocity on the grid centerline follows similar curves for both turbulence models.

Another way to look at the problem is to observe the development of the jet centerline velocity in time. Fig. 5 shows gas velocities on jet centreline for oblique and grid aligned case. The Deardorff model and the SPH method is used here. The discretization interval is 4 cm. Important difference between Figs 4 and 5 is that in the former, the velocities are time averaged, while in the latter the velocities are instantaneous. Fig. 5 shows clearly, that the velocities in both the oblique and grid aligned case are nearly identical in the beginning of the simulation. However the oblique case quickly turns turbulent. This explains the differences seen in Fig. 4a). On coarse grids the grid aligned cases stay relatively laminar while the velocity in the grid aligned case fluctuates strongly. This increased turbulence in the aligned case is possibly the reason for the faster decay of the oblique jets. While there are differences between the two turbulence models it is notable that the differences between the oblique and grid aligned cases remain for both models. Furthermore, grid convergence, insofar as there is any, seems very slow.

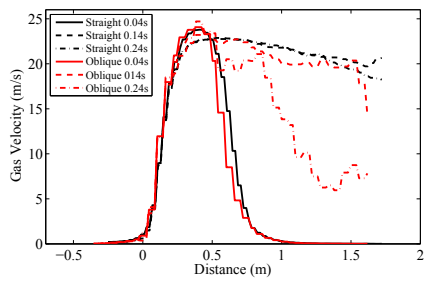


Figure 5: Gas velocities at spray jet centerline at different times. Red lines correspond to oblique jets while black lines correspond to grid aligned jets.

## 6 Conclusions

Both large and small scale simulations of water mist systems were conducted. Good agreement between simulations and experiments was obtained in the near field simulations, but the reproducing the large scale flow pattern of a complex

spray head was found to be very challenging. Reasons for these results were then explored and possible causes were identified. The problems in the large scale simulations can be traced back to problems with simulating oblique sprays. Two kinds of numerical problems were identified. First problem was the proper distribution of momentum source terms in the near field of the spray. It was proposed that this problem can be mitigated by using a higher order interpolation of momentum source terms. The second problem is related to faster dissipation of oblique sprays. It was demonstrated that the issue is likely to be related to turbulence modeling. It is the authors' view that these problems are not specific to the simulation software used and we believe that other structured grid solvers would give similar results.

## Acknowledgements

The experimental data used in this paper is a result of Fire Suppression RD project carried out by VTT Technical Research Centre of Finland and Tampere University of Technology during 2008-2010. This work was sponsored by Marioff Corporation Oy.

## References

[1] Prasad, K., Li, C. & Kailasanath, K., Simulation of water mist suppression of small scale methanol liquid pool fires. *Fire Safety Journal*, **33(3)**, pp. 185–212, 1999.

[2] Prasad, K., Patnaik, G. & Kailasanath, K., A numerical study of water-mist suppression of large scale compartment fires. *Fire Safety Journal*, **37(6)**, pp. 569–589, 2002.

[3] Shimizu, H., Tsuzuki, M., Yamazaki, Y. & Koichi Hayashi, A., Experiments and numerical simulation on methane flame quenching by water mist. *Journal of Loss Prevention in the Process Industries*, **14(6)**, pp. 603–608, 2001.

[4] Nmira, F., Consalvi, J., Kaiss, A., Fernandezpello, A. & Porterie, B., A numerical study of water mist mitigation of tunnel fires. *Fire Safety Journal*, **44(2)**, pp. 198–211, 2009.

[5] Kim, S.C. & Ryou, H.S., An experimental and numerical study on fire suppression using a water mist in an enclosure. *Building and Environment*, **38(11)**, pp. 1309–1316, 2003.

[6] Kim, S.C. & Ryou, H.S., The Effect of Water Mist on Burning Rates of Pool Fire. *Journal of Fire Sciences*, **22(4)**, pp. 305–323, 2004.

[7] Hart, R., *Numerical modelling of tunnel fires and water mist suppression*. Phd thesis, University of Nottingham., 2006.

[8] Husted, B., *Experimental measurements of water mist systems and implications for modelling in CFD*. Ph.D. thesis, Lund University, 2007.

[9] McGrattan, K.B., Hostikka, S., Floyd, J.E., Mell, W.E. & McDermott, R., Fire Dynamics Simulator, Technical Reference Guide, Volume 1: Mathematical Model. NIST Special Publication 1018, National Institute of Standards and Technology, Gaithersburg, Maryland, 2007.
[10] Garg, R., Narayanan, C., Lakehal, D. & Subramaniam, S., Accurate numerical estimation of interphase momentum transfer in lagrangian–eulerian simulations of dispersed two-phase flows. *International Journal of Multiphase Flow*, **33(12)**, pp. 1337–1364, 2007.
[11] Garg, R., Narayanan, C. & Subramaniam, S., A numerically convergent lagrangian–eulerian simulation method for dispersed two-phase flows. *International Journal of Multiphase Flow*, **35(4)**, pp. 376–388, 2009.
[12] Vaari J, S.T., Hostikka S & A, P., Numerical simulations on the performance of water-based fire suppression systems . VTT TECHNOLOGY 54, VTT Technical Research Centre of Finland, Espoo, Finland, 2012.
[13] Moin, P., Squires, K., Cabot, W. & Lee, S., A dynamic subgrid-scale model for compressible turbulence and scalar transport. *Physics of Fluids A: Fluid Dynamics*, **3(11)**, pp. 2746–2757, 1991.
[14] Germano, M., Piomelli, U., Moin, P. & Cabot, W.H., A dynamic subgrid-scale eddy viscosity model. *Physics of Fluids A: Fluid Dynamics*, **3(7)**, pp. 1760–1765, 1991.
[15] Deardorff, J.W., Numerical investigation of neutral and unstable planetary boundary layers. *Journal of Atmospheric Sciences*, **29**, pp. 91–115, 1972.